Thermal fluctuation correction to magnetization and specific heat of vortex solids in type-II superconductors

Dingping Li* and Baruch Rosenstein†

National Center for Theoretical Sciences and Electrophysics Department, National Chiao Tung University, Hsinchu 30050, Taiwan, Republic of China

A systematic calculation of magnetization and specific heat contributions due to fluctuations of vortex lattice in strongly type-II superconductors to precision of 1% is presented. We complete the calculation of the two loop low temperature perturbation theory by including the umklapp processes. Then the Gaussian variational method is adapted to calculation of thermodynamic characteristics of the two-dimensional and the three-dimensional vortex solids in high magnetic field. Based on it as a starting point for a perturbation theory we calculate the leading correction providing simultaneously an estimate of precision. The results are compared to existing nonperturbative approaches.

I. INTRODUCTION

Existence of a vortex lattice in type-II superconductors in magnetic field was predicted by Abrikosov and subsequently observed in various materials ranging from metals to high T_c cuprates. In the original treatment the mean field Ginzburg–Landau (GL) theory, which neglects thermal fluctuations of the vortex matter, was used. Thermal fluctuations are expected to play a much larger role in high T_c superconductors than in the low temperature ones, because the Ginzburg parameter Gi characterizing fluctuations is much larger.[1] In addition, the presence of a strong magnetic field and strong anisotropy in superconductors like BSCCO effectively reduces their dimensionality, thereby further enhancing effects of thermal fluctuations. Under these circumstances fluctuations make the lattice softer, in turn influencing various physical properties like magnetization and specific heat. Eventually it leads to melting of the vortex lattice into a vortex liquid far below the mean field phase transition line.[2,1] The first order melting transition was clearly demonstrated in both magnetization[3] and specific heat experiments.[4] To develop a theory of these fluctuations, even in the case of lowest Landau level (LLL), corresponding to regions of the phase diagram "close" to H_{c2}, is a very nontrivial task and several different approaches were developed.

At the high temperature end (namely far above the mean field transition temperature and thereby in the "vortex liquid" phase) one can develop the traditional "loop" expansion. Since the melting line lies below the mean field line, Thouless and Ruggeri[5,6] proposed a perturbative expansion which can be defined below this line. It contains one loop together with a certain class of higher loop diagrams ("bubbles") and therefore is "nonperturbative." It was shown in field theory that summation of all the bubble diagrams is equivalent to the Gaussian variational approach.[7] In this approach one searches for a "Gaussian" state having the lowest energy. The series provides accurate results at high temperatures, but become inapplicable for LLL dimensionless temperature $a_T \sim (T-T_{mf}(H))/(TH)^{1/2}$ smaller than 2 in 2D and for $a_T \sim (T-T_{mf}(H))/(TH)^{2/3}$ smaller than 1 in

3D, both quite far above the melting line. Generally, attempts to extend the theory to lower temperature by Padé extrapolation were not successful.[8] It is in fact doubtful whether the perturbative results based on Gaussian approximation assuming translational invariant liquid state should be attempted at low a_T.

In Ref. 9, it was shown that below $a_T < -5$ different Gaussian states which are no longer translationally invariant have lower energy. We will present the detailed calculation here (optimized perturbation theory was used to study for liquid state, see Refs. 9 and 10). It is in general a very nontrivial problem to find an inhomogeneous solutions of the corresponding "gap equation" (see Sec. IV). However, using previous experience with low temperature perturbation theory,[11,12] the problem can be significantly simplified and solved using rapidly convergent "modes" expansion. A consistent perturbation theory should start from these states.[13] We then generalize the approach of Ref. 5 by setting up a perturbation theory around the Gaussian Abrikosov lattice state.

Magnetization and specific heat contributions due to vortex lattices are calculated in perturbation theory around this state to next to leading order. This allows to estimate the precision of the calculation. It is the worst, about 1%, near the melting point at $a_T = -10$ and becomes better for lower a_T. At low temperature the result is consistent with the first principles low temperature perturbation theory advanced recently to the two loop order.[11,12] The previous two loop calculation is completed by including the Umklapp processes. One can make several definitive qualitative conclusions using the improved accuracy of the results. The LLL scaled specific heat monotonously rises from its mean field value of $1/\beta_A$ at $a_T = -\infty$ to a slightly higher value of $1.05/\beta_A$ where $\beta_A = 1.16$ is Abrikosov parameter. This is at variance with theory Ref. 14 which uses completely different ideas and has a freedom of arbitrarily choosing certain parameters on a 2% precision level. Although we calculate the contribution of the LLL only, corrections due to higher Landau levels calculated earlier in Refs. 15 and 16 using a less sophisticated method can be included.

The paper is organized as follows. The model is defined in Sec. II. In Sec. III a brief summary of existing results and Umklapp corrected two loop perturbative results in both 2D and 3D are given. Gaussian approximation and the mode expansion used is described in Sec. IV. The basic idea of expansion around the best Gaussian state is explained in Sec. V. The leading corrections are calculated. Results are presented and compared with perturbation theory and other theories in Sec. VI together with conclusions.

II. MODELS

To describe fluctuations of order parameter in thin films or layered superconductors one can start with the Ginzburg–Landau free energy

$$F = L_z \int d^2x \frac{\hbar^2}{2m_{ab}} |D\psi|^2 - a|\psi|^2 + \frac{b'}{2}|\psi|^4, \qquad (1)$$

where $\mathbf{A} = (By, 0)$ describes a constant magnetic field (considered nonfluctuating) in Landau gauge and covariant derivative is defined by $\mathbf{D} \equiv \nabla - i(2\pi/\Phi_0)\mathbf{A}$, $\Phi_0 \equiv hc/e^*$. For strongly type-II superconductors like the high T_c cuprates ($\kappa \sim 100$) and not too far from H_{c2} (this is the range of interest in this paper, for the detailed discussion of the range of applicability see Ref. 15) magnetic field is homogeneous to a high degree due to superposition from many vortices. For simplicity we assume $a(T) = \alpha T_c(1-t)$, $t \equiv T/T_c$, although this temperature dependence can be easily modified to better describe the experimental $H_{c2}(T)$. The thickness of a layer is L_z.

Throughout most of the paper we will use the coherence length $\xi = \sqrt{\hbar^2/(2m_{ab}\alpha T_c)}$ as a unit of length and

$$\frac{dH_{c2}(T_c)}{dT} T_c = \frac{\Phi_0}{2\pi\xi^2}$$

as a unit of magnetic field. After the order parameter field is rescaled as $\psi^2 \to (2\alpha T_c/b')\psi^2$, the dimensionless free energy (the Boltzmann factor) is

$$\frac{F}{T} = \frac{1}{\omega} \int d^2x \left[\frac{1}{2}|\mathbf{D}\psi|^2 - \frac{1-t}{2}|\psi|^2 + \frac{1}{2}|\psi|^4 \right]. \qquad (2)$$

The dimensionless coefficient describing the strength of fluctuations is

$$\omega = \sqrt{2\,\text{Gi}}\, \pi^2 t = \frac{m_{ab}b'}{2\hbar^2\alpha L_z}t, \quad \text{Gi} \equiv \frac{1}{2}\left(\frac{32\pi e^2\kappa^2\xi^2 T_c}{c^2h^2 L_z}\right)^2, \qquad (3)$$

where Gi is the Ginzburg number in 2D . When $(1-t-b)/12b \ll 1$, the lowest Landau level (LLL) approximation can be used.[15] The model then simplifies due to the LLL constraint, $-(\mathbf{D}^2/2)\psi = (b/2)\psi$, rescaling $x \to x/\sqrt{b}$, $y \to y/\sqrt{b}$, and $|\psi|^2 \to |\psi|^2\sqrt{b\omega/4\pi}$, one obtains

$$f = \frac{1}{4\pi} \int d^2x \left[a_T|\psi|^2 + \frac{1}{2}|\psi|^4 \right], \qquad (4)$$

where the 2D LLL reduced temperature

$$a_T \equiv -\sqrt{\frac{4\pi}{b\omega}}\frac{1-t-b}{2} \qquad (5)$$

is the only parameter in the theory.[17,5]

For 3D materials with asymmetry along the z axis the GL model takes the form

$$F = \int d^3x \frac{\hbar^2}{2m_{ab}} \left| \left(\nabla - \frac{ie^*}{\hbar c}\mathbf{A} \right)\psi \right|^2 + \frac{\hbar^2}{2m_c}|\partial_z\psi|^2$$

$$+ a|\psi|^2 + \frac{b'}{2}|\psi|^4 \qquad (6)$$

which can be again rescaled into

$$f = \frac{F}{T} = \frac{1}{\omega} \int d^3x \left[\frac{1}{2}|\mathbf{D}\psi|^2 + \frac{1}{2}|\partial_z\psi|^2 - \frac{1-t}{2}|\psi|^2 + \frac{1}{2}|\psi|^4 \right], \qquad (7)$$

by $x \to \xi x$, $y \to \xi y$, $z \to \xi z/\gamma^{1/2}$, $\psi^2 \to (2\alpha T_c/b')\psi^2$, where $\gamma \equiv m_c/m_{ab}$ is anisotropy. The Ginzburg number is now given by

$$\text{Gi} \equiv \frac{1}{2}\left(\frac{32\pi e^2\kappa^2\xi T_c\gamma^{1/2}}{c^2h^2}\right)^2. \qquad (8)$$

Within the LLL approximation, and rescaling $x \to x/\sqrt{b}$, $y \to y/\sqrt{b}$, $z \to z(b\omega/4\pi\sqrt{2})^{-1/3}$, $\psi^2 \to (b\omega/4\pi\sqrt{2})^{2/3}\psi^2$, the dimensionless free energy becomes

$$f = \frac{1}{4\pi\sqrt{2}} \int d^3x \left[\frac{1}{2}|\partial_z\psi|^2 + a_T|\psi|^2 + \frac{1}{2}|\psi|^4 \right]. \qquad (9)$$

The 3D reduced temperature is

$$a_T = -\left(\frac{b\omega}{4\pi\sqrt{2}}\right)^{-2/3}\frac{1-t-b}{2}. \qquad (10)$$

From now on we work with rescaled quantities only and relate them to measured quantities in Sec. V.

III. PERTURBATION THEORIES AND EXISTING NONPERTURBATIVE RESULTS

A variety of perturbative as well as nonperturbative methods have been used to study this seemingly simple model. There are two phases. Neglecting thermal fluctuations, one obtains the lowest energy configuration $\psi = 0$ for $a_T > 0$ and

$$\psi = \sqrt{-\frac{a_T}{\beta_A}}\varphi,$$

$$\varphi = \sqrt{\frac{2\pi}{\sqrt{\pi}a_\Delta}} \sum_{l=-\infty}^{\infty} \exp\left\{ i\left[\frac{\pi l(l-1)}{2} + \frac{2\pi}{a_\Delta}lx \right] - \frac{1}{2}\left(y - \frac{2\pi}{a_\Delta}l \right)^2 \right\} \qquad (11)$$

for $a_T<0$, where $a_\Delta=\sqrt{4\pi/\sqrt{3}}$ is the lattice spacing in our units and $\beta_A=1.16$.

A. High temperature expansion in the liquid phase

Homogeneous "vortex liquid" phase (which is not separated from the "normal" phase by a transition) has been studied using high temperature perturbation theory by Thouless and Ruggeri.[5] Unfortunately these asymptotic series (even pushed to a very high orders[18]) are applicable only when $a_T>2$. In order to extend the results to lower a_T, attempts have been made to Padé resum the series[6] imposing a constraint that the result matches the Abrikosov mean field as $a_T\to-\infty$. However, if no matching to the limit is imposed, the perturbative results cannot be significantly improved.[8] Experiments,[3,4] Monte Carlo simulations[19] and nonperturbative Bragg chain approximation[20] all point out that there is a first order melting transition around $a_T=-12$. If this is the case it is difficult to support such a constraint.

B. Low temperature perturbation theory in the solid phase: Umklapp processes

Recently a low temperature perturbation theory around Abrikosov solution Eq. (11) was developed and shown to be consistent up to the two loop order.[11,12,16] Since we will use in the present study the same basis and notations and also will compare to the perturbative results we recount here a few basic expressions. The order parameter field ψ is divided into a nonfluctuating (mean field) part and a small fluctuation

$$\psi(x)=\sqrt{\frac{-a_T}{\beta_A}}\varphi(x)+\chi(x). \tag{12}$$

The field χ can be expanded in a basis of quasi momentum eigenfunctions on LLL in 2D:

$$\varphi_\mathbf{k}=\sqrt{\frac{2\pi}{\sqrt{\pi}a_\Delta}}\sum_{l=-\infty}^{\infty}\exp\left\{i\left[\frac{\pi l(l-1)}{2}+\frac{2\pi(x-k_y)}{a_\Delta}l-xk_x\right]\right.$$
$$\left.-\frac{1}{2}\left(y+k_x-\frac{2\pi}{a_\Delta}l\right)^2\right\}. \tag{13}$$

Then we diagonalize the quadratic term of free energy Eq. (4) to obtain the spectrum. Instead of the complex field χ, two "real" fields O and A will be used,

$$\chi(x)=\frac{1}{\sqrt{2}}\int_\mathbf{k}\frac{\exp[-i\theta_k/2]\varphi_\mathbf{k}(x)}{(\sqrt{2\pi})^2}(O_\mathbf{k}+iA_\mathbf{k}),$$
$$\tag{14}$$
$$\chi^*(x)=\frac{1}{\sqrt{2}}\int_\mathbf{k}\frac{\exp[i\theta_k/2]\varphi_\mathbf{k}^*(x)}{(\sqrt{2\pi})^2}(O_{-\mathbf{k}}-iA_{-\mathbf{k}}),$$

where $\gamma_k=|\gamma_k|\exp[i\theta_k]$ and definition of γ_k (and all other definitions of functions) can be found in Appendix A. The eigenvalues found by Eilenberger in Ref. 21 are

$$\epsilon_A(\mathbf{k})=-a_T\left(-1+\frac{2}{\beta_A}\beta_k-\frac{1}{\beta_A}|\gamma_k|\right),$$
$$\tag{15}$$
$$\epsilon_O(\mathbf{k})=-a_T\left(-1+\frac{2}{\beta_A}\beta_k+\frac{1}{\beta_A}|\gamma_k|\right).$$

where β_k is defined in Appendix A. In particular, when $k\to0$ (Ref. 22),

$$\epsilon_A\approx0.12|a_T||k|^4. \tag{16}$$

The second excitation mode ϵ_O has a finite gap. The free energy to the two loop order was calculated in Ref. 12, however the Umklapp processes were not included in some two loop corrections. These processes correspond to momentum nonconserving (up to integer times inverse lattice constant) four leg vertices [see Appendix A, Eq. (A2)]. We therefore recalculated these coefficients. The result in 2D is [see Figs. 1(a) and 1(b)]

$$f_{\text{eff 2D}}=-\frac{a_T^2}{2\beta_A}+2\log\frac{|a_T|}{4\pi^2}-\frac{19.9}{a_T^2}+c_v, \tag{17}$$

where $c_v=\langle\log[(\epsilon_A(\mathbf{k})\epsilon_O(\mathbf{k})/a_T^2]\rangle=-2.92$. In 3D, similar calculation (extending the one carried in Ref. 11 to Umklapp processes) gives

$$f_{\text{eff 3D}}=-\frac{a_T^2}{2\beta_A}+2.848|a_T|^{1/2}+\frac{2.4}{a_T}. \tag{18}$$

C. Nonperturbative methods

Few nonperturbative methods have been attempted. Tesanovic and co-workers[14] developed a method based on an approximate separation of the two energy scales. The larger contribution (98%) is the condensation energy, while the smaller one (2%) describes motion of the vortices. The result for energy in 2D is

$$f_{\text{eff}}=-\frac{a_T^2U^2}{4}-\frac{a_T^2U}{2}\sqrt{\frac{U^2}{4}+\frac{2}{a_T^2}}+2\text{ arc sinh}\left[\frac{a_TU}{2\sqrt{2}}\right],$$
$$\tag{19}$$
$$U=\frac{1}{2}\left[\frac{1}{\sqrt{2}}+\frac{1}{\sqrt{\beta_A}}+\tanh\left[\frac{a_T}{4\sqrt{2}}+\frac{1}{2}\right]\left(\frac{1}{\sqrt{2}}-\frac{1}{\sqrt{\beta_A}}\right)\right].$$

Corresponding expressions in 3D were also derived.

No melting phase transition is seen since it belongs to the 2% which cannot be accounted for within this approach. There exist several Monte Carlo (MC) simulations of the system.[19] The expression Eq. (19) agrees quite well with high temperature perturbation theory and MC simulations and has been used to fit both magnetization and specific heat experiments,[4] but only the mean field level agrees with low temperature perturbation theory. Expanding Eq. (19) in $1/a_T$, one obtains an opposite sign of the one loop contribution, see Fig. 1(a) and discussion in Sec. VI.

Other interesting nonperturbative methods include the $1/N$ expansion[23,24] in which the GL model is generalized to

an N component theory and the phenomenological "Bragg chain fluctuation approximation"[20] based on the elasticity theory of the vortex matter.

IV. GAUSSIAN VARIATIONAL APPROACH

A. General anzatz

Gaussian variational approach originated in quantum mechanics and has been developed in various forms and areas of physics.[25,26] In quantum mechanics it consists of choosing a Gaussian wave function which has the lowest energy expectation value. When fermionic fields are present the approximation corresponds to BCS or Hartree–Fock variational state. In scalar field theory one optimizes the quadratic part of the free energy

$$
\begin{aligned}
f &= \int -\frac{1}{2}\phi^a D^{-1}\phi^a + V(\phi^a) \\
&= \int \frac{1}{2}(\phi^a - v^a)G^{-1ab}(\phi^b - v^b) + \widetilde{V}(G, \phi^a) \\
&= K + \widetilde{V}. \quad (20)
\end{aligned}
$$

To obtain "shift" v^a and "width of the Gaussian" G, one minimizes the Gaussian effective free energy,[26] which is an exact upper bound on the energy (see proof in Ref. 25). The result of the Gaussian approximation can be thought of as resummation of all the "cacti" or loop diagrams.[5,7] Further corrections will be obtained in Sec. V by inserting this solution for G and taking more terms in the expansion of Z.

B. 2D Abrikosov vortex lattice

In our case of one complex field one should consider the most general quadratic form

$$
K = \int_{x,y}(\psi^*(x) - v^*(x))G^{-1}(x,y)(\psi(y) - v(y)) + (\psi
$$
$$
- v(x))H^*(\psi - v(x)) + (\psi^* - v^*(x))H(\psi^* - v^*(x)). \quad (21)
$$

Assuming hexagonal symmetry (a safe assumption for the present purpose), the shift should be proportional to the mean field solution Eq. (12), $v(x) = v\varphi(x)$, with a constant v taken real thanks to global U(1) gauge symmetry. On LLL, as in perturbation theory, we will use variables O_k and A_k defined in Eq. (14) instead of $\psi(x)$,

$$
\psi(x) = v\varphi(x) + \frac{1}{\sqrt{2}2\pi}\int_{\mathbf{k}}\exp\left[-\frac{i\theta_{\mathbf{k}}}{2}\right]\varphi_{\mathbf{k}}(x)(O_{\mathbf{k}} + iA_{\mathbf{k}}). \quad (22)
$$

The phase defined after Eq. (14) is quite important for simplification of the problem and was introduced for future convenience. The most general quadratic form is

$$
K = \frac{1}{8\pi}\int_k O_{\mathbf{k}}G_{OO}^{-1}(k)O_{-\mathbf{k}} + A_{\mathbf{k}}G_{AA}^{-1}(k)A_{-\mathbf{k}}
$$
$$
+ O_{\mathbf{k}}G_{OA}^{-1}(k)A_{-\mathbf{k}} + A_{\mathbf{k}}G_{OA}^{-1}(k)O_{-\mathbf{k}}, \quad (23)
$$

with matrix of functions $G(k)$ on Brillouin zone to be determined together with the constant v by the variational principle. The corresponding Gaussian free energy is

$$
\begin{aligned}
f_{\text{Gauss}} &= a_T v^2 + \frac{\beta_A}{2}v^4 - 2 - \langle\log[(4\pi)^2\det(G)]\rangle_k \\
&+ \langle a_T(G_{OO}(k) + G_{AA}(k)) + v^2[(2\beta_k + |\gamma_k|)G_{OO}(k) \\
&+ (2\beta_k - |\gamma_k|)G_{AA}(k)]\rangle_k\langle\beta_{k-l}[G_{OO}(k) + G_{AA}(k)] \\
&\times[G_{OO}(l) + G_{AA}(l)]\rangle_{k,l} + \frac{1}{2\beta_A}\{\langle|\gamma_k|(G_{OO}(k) \\
&- G_{AA}(k))\rangle^2 + 4\langle|\gamma_k|G_{OA}(k)\rangle_k^2\}, \quad (24)
\end{aligned}
$$

where $\langle\cdots\rangle_k$ denotes average over the Brillouin zone. The minimization equations are

$$
\begin{aligned}
v^2 &= -\frac{a_T}{\beta_A} - \frac{1}{\beta_A}\langle(2\beta_k + |\gamma_k|)G_{OO}(k) \\
&+ (2\beta_k - |\gamma_k|)G_{AA}(k)\rangle_k, \quad (25)
\end{aligned}
$$

$$
\begin{aligned}
[G(k)^{-1}]_{OO} &= a_T + v^2(2\beta_k + |\gamma_k|) \\
&+ \left\langle\left(2\beta_{k-l} + \frac{|\gamma_k||\gamma_l|}{\beta_A}\right)G_{OO}(l) \right. \\
&+ \left.\left(2\beta_{k-l} - \frac{|\gamma_k||\gamma_l|}{\beta_A}\right)G_{AA}(k)\right\rangle_l, \quad (26)
\end{aligned}
$$

$$
\begin{aligned}
[G(k)^{-1}]_{AA} &= a_T + v^2(2\beta_k - |\gamma_k|) \\
&+ \left\langle\left(2\beta_{k-l} + \frac{|\gamma_k||\gamma_l|}{\beta_A}\right)G_{AA}(l) \right. \\
&+ \left.\left(2\beta_{k-l} - \frac{|\gamma_k||\gamma_l|}{\beta_A}\right)G_{OO}(k)\right\rangle_l, \quad (27)
\end{aligned}
$$

$$
\begin{aligned}
[G(k)^{-1}]_{OA} &= -\frac{G_{OA}(k)}{G_{OO}(k)G_{AA}(k) - G_{OA}(k)^2} \\
&= 4\frac{|\gamma_k|}{\beta_A}\langle|\gamma_l|G_{OA}(l)\rangle_l. \quad (28)
\end{aligned}
$$

These equations look quite intractable, however they can be simplified. The crucial observation is that after we have inserted the phase $\exp[-i\theta_k/2]$ in Eq. (22) using our experience with perturbation theory, G_{AO} appears explicitly only on the right-hand side of the last equation. It also implicitly appears on the left-hand side due to a need to invert the matrix G. Obviously $G_{OA}(k) = 0$ is a solution and in this case the matrix diagonalizes. However general solution can be shown to differ from this simple one just by a global

gauge transformation. Subtracting Eq. (26) from Eq. (27) and using Eq. (28), we observe that matrix G^{-1} has the form

$$G^{-1} \equiv \begin{pmatrix} E_O(k) & E_{OA}(k) \\ E_{OA}(k) & E_A(k) \end{pmatrix}$$

$$= \begin{pmatrix} E(k)+\Delta_1|\gamma_k| & \Delta_2|\gamma_k| \\ \Delta_2|\gamma_k| & E(k)-\Delta_1|\gamma_k| \end{pmatrix},$$

where Δ_1,Δ_2 are constants. Substituting this into the Gaussian energy one finds that it depends on Δ_1,Δ_2 via the combination $\Delta=\sqrt{\Delta_1^2+\Delta_2^2}$ only. Therefore without loss of generality we can set $\Delta_2=0$, thereby returning to the $G_{OA}=0$ case.[27]

Using this observation the gap equations significantly simplify. The function $E(k)$ and the constant Δ satisfy

$$E(k)=a_T+2v^2\beta_k+2\left\langle \beta_{k-l}\left(\frac{1}{E_O(l)}+\frac{1}{E_A(l)}\right)\right\rangle_l, \quad (29)$$

$$\beta_A \Delta = a_T - 2\left\langle \beta_k\left(\frac{1}{E_O(k)}+\frac{1}{E_A(k)}\right)\right\rangle_k. \quad (30)$$

The Gaussian energy becomes

$$f=v^2a_T+\frac{\beta_A}{2}v^4+f_1+f_2+f_3,$$

$$(31)$$

$$f_1=\left\langle \log\left[\frac{E_O(k)}{4\pi^2}\right]+\log\left[\frac{E_A(k)}{4\pi^2}\right]\right\rangle_k,$$

$$f_2=-2+\left\langle a_T\left(\frac{1}{E_O(k)}+\frac{1}{E_A(k)}\right)+v^2\left[(2\beta_k+|\gamma_k|)\right.\right.$$

$$\left.\left.\times\frac{1}{E_O(k)}+(2\beta_k-|\gamma_k|)\frac{1}{E_A(k)}\right]\right\rangle_k,$$

$$(32)$$

$$f_3=\left\langle \beta_{k-l}\left[\frac{1}{E_O(k)}+\frac{1}{E_A(k)}\right]\left[\frac{1}{E_O(l)}+\frac{1}{E_A(l)}\right]\right\rangle_{k,l}$$

$$+\frac{1}{2\beta_A}\left[\left\langle |\gamma_k|\left(\frac{1}{E_O(k)}-\frac{1}{E_A(k)}\right)\right\rangle_k\right]^2.$$

Using Eq. (29), a formula

$$\beta_k=\sum_{n=0}^{\infty}\chi^n\beta_n(k),$$

$$\beta_n(k)\equiv\sum_{|\mathbf{X}|^2=na_\Delta^2}\exp[i\mathbf{k}\cdot\mathbf{X}]$$

derived in Appendix A and the hexagonal symmetry of the spectrum, one deduces that $E(k)$ can be expanded in "modes"

TABLE I. Mode expansion 2D.

a_T	1 mode	2 modes	3 modes
-1000	$-446\,023.8395$	$-431\,171.9948$	$-431\,171.9757$
-300	$-40\,131.292\,17$	$-38\,796.0277$	$-38\,796.022\,97$
-100	$-4450.416\,36$	$-4303.286\,85$	$-4303.285\,93$
-50	$-1106.515\,75$	$-1070.638\,06$	$-1070.637\,91$
-20	$-171.678\,045$	$-166.690\,727$	$-166.690\,827$
-10	$-39.292\,885$	$-38.433\,571$	$-38.433\,645$
-5	$-7.315\,3440$	$-7.223\,7197$	$-7.223\,7422$

$$E(k)=\sum E_n\beta_n(k). \quad (33)$$

The integer n determines the distance of a points on reciprocal lattice from the origin (see Fig. 4) and $\chi\equiv\exp[-a_\Delta^2/2]=\exp[-2\pi/\sqrt{3}]=0.0265$. One estimates that $E_n\simeq\chi^n a_T$, therefore the coefficients decrease exponentially with n. Note (see Fig. 4) that for some integers, for example, $n=2,5,6$, $\beta_n=0$. Retaining only the first s modes will be called "the s mode approximation." We minimized numerically the Gaussian energy by varying v,Δ and the first few modes of $E(k)$. The sample results for various a_T and number of modes are given in Table I.

We see that in the interesting region of not very low temperatures the energy converges extremely fast. In practice two modes are quite enough. The results for the Gaussian energy are plotted in Fig. 1 and will be compared with other approaches in Sec. VI. Furthermore one can show that around $a_T<-4.6$, the Gaussian liquid energy is larger than the Gaussian solid energy. So naturally when $a_T<-4.6$, one should use the Gaussian solid to set up a perturbation theory. For $a_T>-4.2$, there is no solution for the gap equations.

C. 3D Abrikosov vortex lattice

In 3D, we expand in bases of plane waves in the third direction times previously used quasimomentum function,

$$\psi(\mathbf{x},z)=v\varphi(\mathbf{x})+\frac{1}{\sqrt{2}(2\pi)^{3/2}}\int_{\mathbf{k},k_z}\exp\left[-\frac{i\theta_{\mathbf{k}}}{2}\right]$$

$$\times\varphi_{\mathbf{k}}(\mathbf{x})\exp i(k_z\cdot z)(O_k+iA_k). \quad (34)$$

The quadratic form is

$$K=\frac{1}{8\pi\sqrt{2}}\int_k O_k G_{OO}^{-1}(k)O_{-k}+A_k G_{AA}^{-1}(k)A_{-k}, \quad (35)$$

where integration over k is understood as integration over Brillouin zone and over k_z. Most of the derivation and important observations are intact. The modifications are

$$G_{OO}^{-1}(k) = \frac{k_z^2}{2} + E_O(\mathbf{k}),$$

$$G_{AA}^{-1}(k) = \frac{k_z^2}{2} + E_A(\mathbf{k}).$$

The corresponding Gaussian free energy density (after integration over k_z) is

$$f = v^2 a_T + \frac{\beta_A}{2} v^4 + f_1 + f_2 + f_3,$$

$$f_1 = \langle \sqrt{E_O(\mathbf{k})} + \sqrt{E_A(\mathbf{k})} \rangle_{\mathbf{k}},$$

(36)

$$f_2 = a_T \left\langle \frac{1}{\sqrt{E_O(\mathbf{k})}} + \frac{1}{\sqrt{E_A(\mathbf{k})}} \right\rangle_{\mathbf{k}} + \left\langle v^2 \left[(2\beta_k + |\gamma_k|) \right. \right.$$

$$\left. \times \frac{1}{\sqrt{E_O(\mathbf{k})}} + (2\beta_k - |\gamma_k|) \frac{1}{\sqrt{E_A(\mathbf{k})}} \right]_{\mathbf{k}},$$

(37)

$$f_3 = \left\langle \beta_{k-l} \left[\frac{1}{\sqrt{E_O(\mathbf{k})}} + \frac{1}{\sqrt{E_A(\mathbf{k})}} \right] \left[\frac{1}{\sqrt{E_O(\mathbf{l})}} + \frac{1}{\sqrt{E_A(\mathbf{l})}} \right] \right\rangle_{k,l}$$

$$+ \frac{1}{2\beta_A} \left[\left\langle |\gamma_k| \left(\frac{1}{\sqrt{E_O(\mathbf{k})}} - \frac{1}{\sqrt{E_A(\mathbf{k})}} \right) \right\rangle_k \right]^2.$$

Minimizing the above energy, gap equations similar to that in 2D can be obtained. One finds that

$$E_O(\mathbf{k}) = E(\mathbf{k}) + \Delta |\gamma_k|,$$

$$E_A(\mathbf{k}) = E(\mathbf{k}) - \Delta |\gamma_k|.$$

$E(\mathbf{k})$ can be solved by modes expansion 2D. We minimized numerically the Gaussian energy by varying v, Δ and first few modes of $E(k)$. The sample results of free energy density for various a_T with three modes are given in Table II.

In practice two modes are also quite enough in 3D. As in the case of 2D, one can show that around $a_T < -5.5$, the gaussian liquid energy is larger than the Gaussian solid energy. So naturally when $a_T < -5.5$, one should use the Gaussian solid to set up a perturbation theory in 3D. When around $a_T > -5$, there is no solution for the gap equations.

V. CORRECTIONS TO THE GAUSSIAN APPROXIMATION

In this section, we calculate the lowest order correction to the Gaussian approximation (that will be called post-Gaussian correction), which will determine the precision of the Gaussian approximation. This is necessary in order to fit experiments and compare with low temperature perturbation theory and other nonperturbative methods.

First we review a general idea behind calculating systematic corrections to the Gaussian approximation.[25] The procedure is rather similar to calculating corrections to the Hartree–Fock approximations used in fermionic systems. Gaussian variational principle provided us with the best (in a certain sense) quadratic part of the free energy K from which the "steepest descent" corrections can be calculated. The free energy is divided into the quadratic part and a "small" perturbation $\tilde{V}$. For a general scalar theory defined in Eq. (20) it takes the form

$$f = K + \alpha \tilde{V},$$

$$K = \frac{1}{2} \phi^a G^{-1ab} \phi^b.$$

(38)

$$\tilde{V} = -\frac{1}{2} \phi^a D^{-1} \phi^a + V(\phi^a) - \frac{1}{2} \phi^a G^{-1ab} \phi^b.$$

Here the auxiliary parameter α was introduced to set up a perturbation theory. It will be set to one at the end of the calculation. Expanding the logarithm of the statistical sum in powers of α,

$$Z = \int \mathcal{D}\phi^a \exp(-K) \exp(-\alpha \tilde{V})$$

$$= \int \mathcal{D}\phi^a \sum_{n=0}^{\infty} \frac{1}{n!} (\alpha \tilde{V})^n \exp(-K),$$

(39)

one retains only the first few terms. It was shown in Ref. 26 that generally only two-particle irreducible diagrams contribute to the post-Gaussian correction. The Gaussian approximation corresponds to retaining only the first two terms, $n = 0,1$, while the post-Gaussian correction retains in addition the contribution of order α^2.

Feynman rules in our case are shown in Fig. 5. We have two propagators for fields A and O and three and four leg vertices. Using these rules the postgaussian correction is presented on Fig. 6 as a set of two and three loop diagrams. The corresponding expressions are given in Appendix B. The Brillouin zone averages were computed numerically using the three modes gaussian solution of the previous section. Now we turn to discussion of the results.

TABLE II. Mode expansion 3D.

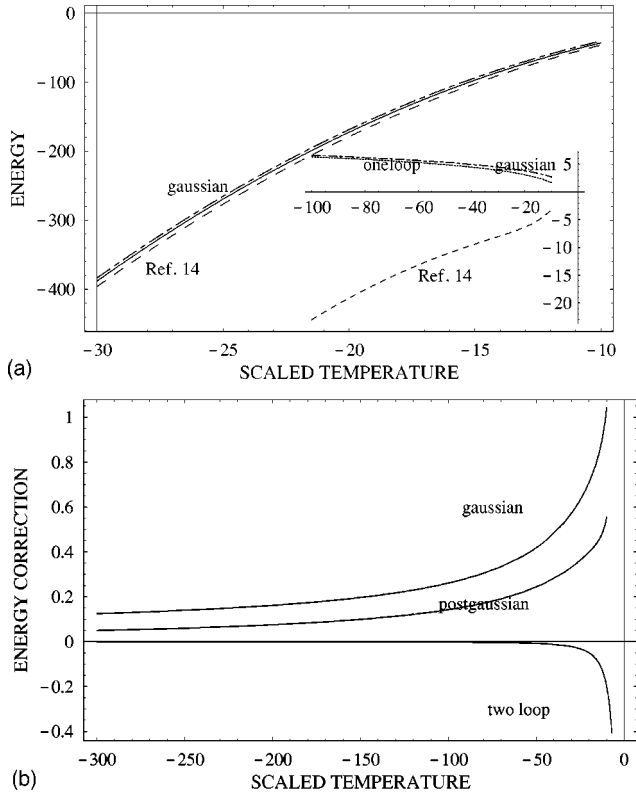| a_T	-300	-100	-50	-30	-20	-10	-5.5
f	$-38\,757.2294$	-4283.2287	-1057.6453	-372.2690	-159.5392	-33.9873	-6.5103

(a)

(b)

FIG. 1. Scaled free energy of vortex solid. From top to bottom, Gaussian approximation (dashed–dotted line), mean field (solid line), theory Ref. 14 (dashed line). Inset, corrections to mean field calculated using (from top to bottom) Gaussian (dashed–dotted line), one loop perturbation theory (dotted line), and theory Ref. 14 (dashed line). (b) More refined comparison of different approximations to free energy. Mean field as well as the one loop perturbative contributions are subtracted.

VI. RESULTS, COMPARISON WITH OTHER APPROACHES AND CONCLUSION

Results for LLL scaled energy, magnetization and specific heat in 2D are presented in Figs. 1, 2, and 3, respectively.

A. Energy

The Gaussian energy provides a rigorous upper bound on free energy.[25] Figure 1(a) shows the 2D Gaussian energy (the dashed–dotted line), which in the range of a_T from -30 to -10 is just above the mean field (the solid gray line). This is because it correctly accounts for the (positive) logarithmic one loop correction of Eq. (17). In contrast the results of the theory by Tesanovic *et al.*[14] (the dashed gray line) are lower than the mean field. This reflects the fact that although the correct large $|a_T|$ limit is built in, the expansion of the expression Eq. (19) gives negative coefficient of the $\log|a_T|$ term. This is inconsistent with both the low temperature perturbation theory and the Gaussian approximation. The difference between this theory and our result is smaller than 2% only when $a_T < 30$ or at small a_T below the 2D melting line (which occurs at $a_T = -13$ according to Monte Carlo[19] and
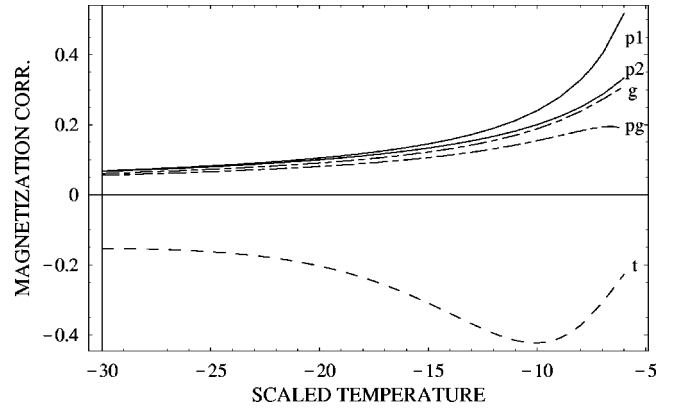

FIG. 2. Thermal fluctuations correction to magnetization of vortex solid. From top to bottom, one and two loop perturbation theory (solid lines p1 and p2, respectively), Gaussian and post-Gaussian approximations (dashed–dotted lines g and pg, respectively), theory Ref. 14 (dashed line, t).

phenomenological estimates[18,1]) where the lines become closer again. It never gets larger than 10% though. To effectively quantitatively study the model one has to subtract the dominant mean field contribution. This is done in the inset of Fig. 1(a). We plot the gaussian result (the dashed–dotted line), the one loop perturbative result (the solid line) and Eq. (19) (the dashed gray line) in an expanded region $-100 < a_T < -10$. The Gaussian approximation is a bit higher than the one loop.

To determine the precision of the Gaussian approximation and compare with the perturbative two loop result, we further subtracted the one loop contribution on Fig. 1(b). As expected the post-Gaussian result is lower than the Gaussian though higher than the two loop. The difference between the Gaussian and the post-Gaussian approximation in the region shown is about $|\Delta f| = 0.2$, which translates into 0.2% at $a_T = -30$, 0.4% at $a_T = -20$ and 2% at $a_T = -12$. The fit for
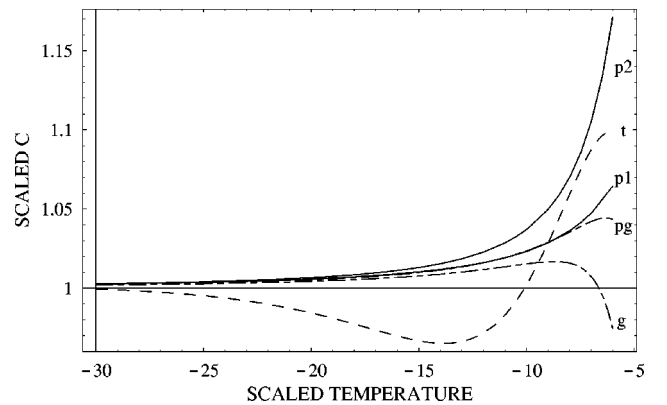

FIG. 3. Scaled specific heat Eq. (45) normalized by the mean field. One and two loop perturbation theory (solid lines p1 and p2, respectively), Gaussian and post-Gaussian approximations (dashed–dotted lines g and pg, respectively), theory Ref. 14 (dashed line, t).

the Gauss and post-Gaussian energy in the region $-30 < a_T < -6$ are

$$f_{g2D} = -\frac{a_T^2}{2\beta_A} + 2\log|a_T| + 0.119 - \frac{19.104}{a_T}$$
$$-\frac{60.527\log|a_T|}{a_T^2} + \frac{36.511}{a_T^2} + c_v,$$

$$f_{pg2D} = -\frac{a_T^2}{2\beta_A} + 2\log|a_T| + 0.068 - \frac{11.68}{a_T}$$
$$-\frac{60.527\log|a_T|}{a_T^2} + \frac{38.705}{a_T^2} + c_v.$$

In 3D, similarly one found that

$$f_{g3D} = -\frac{a_T^2}{2\beta_A} + 2.848\,35|a_T|^{1/2} + \frac{3.1777}{a_T}$$
$$-\frac{0.8137\log^2[-a_T]}{a_T}. \tag{40}$$

B. Magnetization

The dimensionless LLL magnetization is defined as

$$m(a_T) = -\frac{df_{\text{eff}}(a_T)}{da_T} \tag{41}$$

and the measure magnetization is

$$4\pi M = -\frac{e^*h}{cm_{ab}}\langle|\psi|^2\rangle = -\frac{e^*h}{cm_{ab}}|\psi_r|^2 \frac{b'}{2\alpha T_c}\sqrt{\frac{b\omega}{4\pi}}, \tag{42}$$

where ψ is the order parameter of the original model, and ψ_r is the rescaled one, which is equal to $df_{\text{eff}}(a_T)/da_T$. Thus

$$4\pi M = \frac{e^*h}{cm_{ab}} \frac{b'}{2\alpha T_c}\sqrt{\frac{b\omega}{4\pi}}m(a_T). \tag{43}$$

We plot the scaled magnetization in region $-30 < a_T < -6$. Again, the mean field contribution dominates, so we subtract it in Fig. 2. The solid line is the one loop approximation, while the gray line is the two loop approximation. At small negative a_T the postgaussian (the upper gray dashed–dotted line) is very close to the two loop result, while the Gaussian approximation (the dashed–dotted line) is a bit lower. All of these lines are above mean field. On the other hand, the result of Ref. 14 (the gray dashed line) is below the mean field. Magnetization jump at the melting point is smaller than our precision of 2% at $a_T = -12$. Our result for the Gaussian magnetization and the post-Gaussian correction in this range can be conveniently fitted with

$$m_{g2D} = \frac{a_T}{\beta_A} - \frac{2}{a_T} - \frac{19.10}{a_T^2} + \frac{133.55}{a_T^3} - \frac{121.05\log[-a_T]}{a_T^3},$$

$$\Delta m_{pg2D} = \frac{7.525}{a_T^2} - \frac{59.15}{a_T^3} + \frac{43.64\log[-a_T]}{a_T^3},$$

respectively.

Similar discussion for the case of 3D can be deduced from Eqs. (41), Eq. (40), and

$$4\pi M = -\frac{e^*h}{cm_{ab}}\langle|\psi|^2\rangle = -\frac{e^*h}{cm_{ab}}|\psi_r|^2 \frac{b'}{2\alpha T_c}\left(\frac{b\omega}{4\pi\sqrt{2}}\right)^{2/3}$$
$$= \frac{e^*h}{cm_{ab}} \frac{b'}{2\alpha T_c}\left(\frac{b\omega}{4\pi\sqrt{2}}\right)^{2/3}m(a_T), \tag{44}$$

where the Gaussian scaled magnetization can be obtained by differentiation of Eq. (40). We did not attempt to calculate the post-Gaussian correction in 3D.

C. Specific heat

The scaled LLL specific heat is defined as

$$c(a_T) = -\frac{d^2f_{\text{eff}}(a_T)}{da_T^2} \tag{45}$$

and the original specific heat is related to the scaled specific heat c in 2D via

$$C = \frac{1}{4\pi\xi^2 T}\left[-b + \sqrt{\frac{\pi\hbar^2\alpha bT_c}{2m^*b'T}}\frac{-3t-1+b}{2}m(a_T)\right.$$
$$\left. + \frac{\pi\hbar^2\alpha T_c}{m^*b'T}\frac{(-t-1+b)_2}{2}c(a_T)\right].$$

We plot the scaled specific heat divided by the mean field value $c_{mf} = 1/\beta_A$ in the range $-30 < a_T < -6$ on Fig. 3. The solid line is one loop approximation, while the gray line is the two loop approximation. At large $|a_T|$ the post-Gaussian (gray dashed–dotted line) is very closed to the one loop result. Finally the Gaussian approximation (dashed–dotted line) is a bit lower. All these lines are slightly above mean field. On the contrary, the result of Ref. 14 (dashed gray line) is below the mean field. Our Gaussian result and its correction in this range can be conveniently fitted with

$$\frac{c_g}{c_{mf}} = 1 + \beta_A\left(\frac{2}{a_T^2} + \frac{38.2}{a_T^3} - \frac{521.7}{a_T^4} + \frac{363.2\ln[-a_T]}{a_T^4}\right)$$

$$\frac{\Delta c_g}{c_{mf}} = \beta_A\left(-\frac{15.05}{a_T^3} + \frac{221.1}{a_T^4} - \frac{130.9\ln[-a_T]}{a_T^4}\right).$$

Qualitatively the Gaussian specific heat is consistent with experiments[4] which show that the specific heat first raise before dropping sharply beyond the melting point.
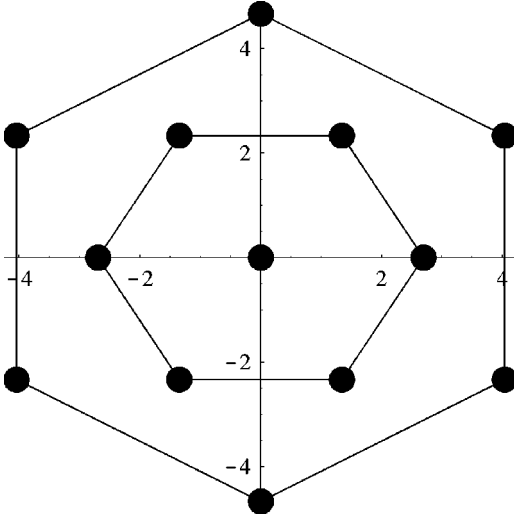
FIG. 4. Reciprical hexagonal lattice points **X** belonging to three lowest order "stars" in the mode expansion of β_k.

D. Conclusions

In this paper, we applied the Gaussian variational principle to the problem of thermal fluctuations in vortex lattice state. Then the correction to it was calculated perturbatively. This generalizes corresponding treatment of fluctuations in the homogeneous phase (vortex liquid) by Thouless and co-workers.[5] Also Umklapp processes were included in the low temperature two loop perturbation theory expression. The results of Gaussian perturbative and some nonperturbative approaches were compared. The perturbative corrections (up to two loop) already show that the expression of the theory of Ref. 14 with the mean field subtracted has wrong sign. The Gaussian approximation provides a rigorous lower bound and is superior over the one loop result. It is valid even in the region in which the one loop diverges. In particular the end of point below which the overheated solid exists as a metastable state is estimated at $a_T = -4.6$. Similarly the corrected Gaussian approximation is an improvement over the two loop result in the temperature range near the melting line. The calculation of the post-Gaussian correction allows us to estimate the precision, for example, the specific heat precision is higher than 1% for $-20 < a_T < -6$ (the melting line is located at $a_T = -12$) and higher than 0.1% for $a_T < -20$. The specific heat of the vortex solid is predicted to be monotonic (unlike the theory of Ref. 14 where there is a minimum followed by a maximum) consistent with several experiments.[4] We hope that increased sensitivity of both magnetization and specific heat experiments will test the precision of the theory (see Fig. 3).

ACKNOWLEDGMENTS

APPENDIX A

In this Appendix the basic definitions are collected. Brillouin zone averages of products of four quasimomentum functions are defined by

$$\beta_k = \langle |\varphi|^2 \varphi_{\vec{k}} \varphi_{\vec{k}}^* \rangle,$$

$$\gamma_k = \langle (\varphi^*)^2 \varphi_{-\vec{k}} \varphi_{\vec{k}} \rangle, \tag{A1}$$

$$\gamma_{k,l} = \langle \varphi_k^* \varphi_{-k}^* \varphi_{-\vec{l}} \varphi_{\vec{l}} \rangle.$$

We also need a more general product $\langle \varphi_{k_1}^* \varphi_{k_2} \varphi_{k_3}^* \varphi_{k_4} \rangle$ in order to calculate post-Gaussian corrections. This is just a perturbative four-leg vertex,

$$\langle \varphi_{k_1}^* \varphi_{k_2} \varphi_{k_3}^* \varphi_{k_4} \rangle = \exp\left[\frac{i\pi^2}{2}(n_1^2 - n_1) + i\frac{2\pi}{a_\Delta} n_1 k_{3y} \right] \delta^q[\mathbf{k}_1 - \mathbf{k}_2 + \mathbf{k}_3 - \mathbf{k}_4] \lambda[\mathbf{k}_1 - \mathbf{k}_2, \mathbf{k}_2 - \mathbf{k}_4],$$

$$\tag{A2}$$

$$\lambda[\mathbf{l}_1, \mathbf{l}_2] = \sum_{\mathbf{Q}} \exp\left[-\frac{|\mathbf{l}_1 + \mathbf{Q}|^2}{2} + i(l_{1x} + l_{2x})Q_y - i(l_{1y} + l_{2y})Q_x \right] \exp[i(l_{1x} + l_{2x})l_{1y}],$$

where **Q** are reciprocal lattice vectors,

$$\mathbf{Q} = m_1 \tilde{\mathbf{d}}_1 + m_2 \tilde{\mathbf{d}}_2. \tag{A3}$$

Here $\mathbf{k}_1 - \mathbf{k}_2 + \mathbf{k}_3 - \mathbf{k}_4 = n_1 \tilde{\mathbf{d}}_1 + n_2 \tilde{\mathbf{d}}_2$ is assumed and the basis of reciprocal lattice is $\tilde{\mathbf{d}}_1 = (2\pi/a_\Delta)[1, -(1/\sqrt{3})]$, $\tilde{\mathbf{d}}_2 = [0, (4\pi/a_\Delta\sqrt{3})]$, $a_\Delta = \sqrt{4\pi/\sqrt{3}}$. It is dual to the lattice $\mathbf{e}_1 = (a_\Delta, 0)$, $\mathbf{d}_2 = [(a_\Delta/2), (a_\Delta\sqrt{3}/2)]$. When $\mathbf{k}_1 - \mathbf{k}_2 + \mathbf{k}_3 - \mathbf{k}_4 \neq n_1 \tilde{\mathbf{d}}_1 + n_2 \tilde{\mathbf{d}}_2$ the quantity vanishes. The delta function differs from the Kroneker,

$$\delta^q[\mathbf{k}] = \sum_{\mathbf{Q}} \delta[\mathbf{k} + \mathbf{Q}].$$

From the above formula, one gets the following expansion of β_k:

$$\beta_k = \sum_{m_1, m_2} \exp\left[-\frac{|\mathbf{X}|^2}{2} + i\mathbf{k} \cdot \mathbf{X} \right] = \sum_n \exp\left[-\frac{a_\Delta^2}{2} n \right] \beta_n(k),$$

$$\tag{A4}$$

where $\mathbf{X} = n_1 \mathbf{d}_1 + n_2 \mathbf{d}_2$.

To simplify the minimization equations we used the following general identity. Any sixfold (D_6) symmetric function $F(k)$ [namely a function satisfying $F(k) = F(k')$, where k, k' is related by a $2\pi/6$ rotation] obeys

$$\int_k F(k) \gamma_k \gamma_{k,l} = \frac{\gamma_l}{\beta_A} \int_k F(k) |\gamma_k|^2, \tag{A5}$$

where γ_k and $\gamma_{k,l}$ are defined in Eq. (A1). This can be seen by expanding F in Fourier modes and symmetrizing.
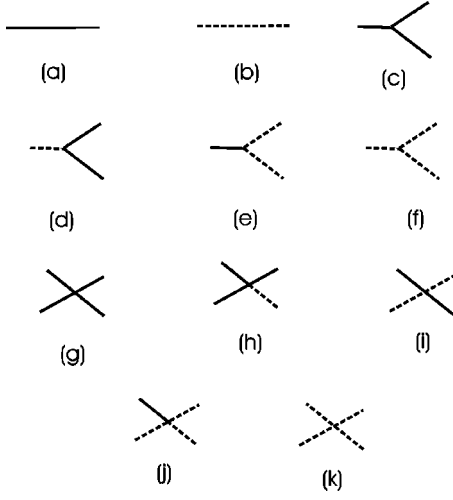
FIG. 5. Feynman rules of the low temperature perturbation theory. The solid line (a) denoted the O mode propagator, while the dashed line (b) denotes the A mode propagator. Various three leg and four leg vertices are presented in (c)–(f) and (g)–(k), respectively.

APPENDIX B

In this Appendix we specify Feynman rules and collect expressions for diagrams. The solid line Fig. 5(a) represents O and the dashed line Fig. 5(b) represents A. Figure 5(c) is a vertex with three O. In the coordinate space, it is $2v[\varphi O(O^+)^2 + \text{c.c.}]$. Figure 5(c) is $-2iv\varphi^+ O^2 A^+ - 4iv\varphi OO^+ A^+ + \text{c.c}$, Fig. 5(g) is $\frac{1}{2}|O(x)|^4$, Fig. 5(h) is $2OO^+(AO^+ - OA^+)$, and Fig. 5(i) is $4OO^+AA^+ - [O^2(A^+)^2 + \text{c.c.}]$.

Other vertices, for example, formulas for diagrams in Fig. 5(e), 5(f), 5(j), and 5(k), can be obtained by substituting $O \rightarrow iA, A \rightarrow -iO$ from formulas for diagrams in Fig. 5(d), 5(c), 5(h), and 5(g), respectively.

The propagator in coordinate space can be written as

$$\langle O^+(x)O^+(y)\rangle = 4\pi\int_{\mathbf{k}} E_O(k)\varphi_k^*(x)\varphi_{-k}^*(y) = 4\pi P_O^+(x,y),$$

$$\langle O(x)O(y)\rangle = 4\pi\int_{\mathbf{k}} E_O(k)\varphi_k(x)\varphi_{-k}(y) = 4\pi P_O^-(x,y),$$

$$\text{(B1)}$$

$$\langle O(x)O^+(y)\rangle = 4\pi\int_{\mathbf{k}} E_O(k)\varphi_k(x)\varphi_k^*(y) = 4\pi P_O(x,y).$$

Functions $P_A^+(x,y), P_A^-(x,y), P_A(x,y)$ can be defined similarly.

One finds three loops contribution to free energy from two $OOOO$ vertex contraction, see Fig. 6(a), $-1/16(2\pi)^5\int_{\mathbf{x}}\langle f_{oooo}\rangle_{\mathbf{y}}$,

$$f_{oooo} = 4\langle|P_O|^4 + |P_O^+|^4 + 4|P_O P_O^+|^2\rangle_{\mathbf{y}}. \quad \text{(B2)}$$

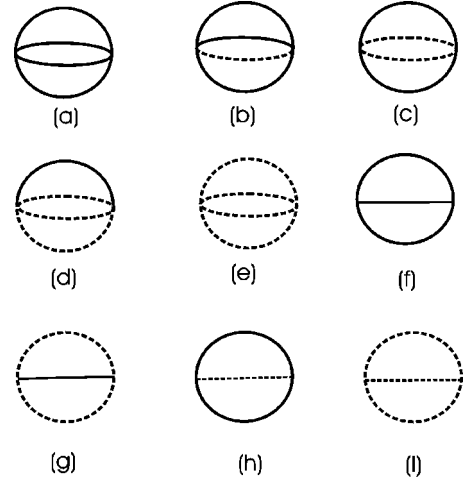Coordinates are not written explicitly since all of them are the same $P_O(x,y)$, etc.

FIG. 6. Contributions to the post-Gaussian correction to free energy.

The contribution from the diagrams in Fig. 6(b) is $-1/16(2\pi)^5\int_{\mathbf{x}}\langle f_{oooa}\rangle_{\mathbf{y}}$, and

$$f_{oooa} = |P_O|^2(-16P_O^+ P_A^- + 8P_O P_A^*) + |P_O^+|^2(-8P_O^+ P_A^-$$
$$+ 16P_O P_A^*) + \text{c.c.} \quad \text{(B3)}$$

The diagrams in Fig. 6(c) are $-1/16(2\pi)^5\int_{\mathbf{x}}\langle f_{ooaa}\rangle_{\mathbf{y}}$ and

$$f_{ooaa} = 16(|P_O|^2 + |P_O^+|^2)(|P_A|^2 + |P_A^+|^2) + 4([P_O^+]^2[P_A^-]^2$$
$$+ P_O^2[P_A^2]^* + \text{c.c.}) - 32(P_O P_O^* P_A^+ P_A + \text{c.c.}). \quad \text{(B4)}$$

The diagrams in Fig. 6(f) are $-v^2/16(2\pi)^4\int_{\mathbf{x}}\langle f_{ooo}\rangle_{\mathbf{y}}$ and

$$f_{ooo} = |P_O|^2(16P_O^+ \varphi(x)\varphi(y) + 8P_O^* \varphi(x)\varphi^*(y) + \text{c.c.})$$
$$+ |P_O^+|^2(8P_O^+ \varphi(x)\varphi(y) + 16P_O^* \varphi(x)\varphi^*(y) + \text{c.c.}).$$
$$\text{(B5)}$$

The diagrams in Fig. 6(h) are $-v^2/16(2\pi)^4\int_{\mathbf{x}}\langle f_{ooa}\rangle_{\mathbf{y}}$ and

$$f_{ooa} = -8(P_O^-)^2 P_A^+ \varphi^*(x)\varphi^*(y) - 16(|P_O|^2 + |P_O^+|^2)$$
$$\times (P_A^+ \varphi(x)\varphi(y) - P_A \varphi^*(x)\varphi(y))$$
$$+ 8P_O^2 P_A^* \varphi^*(x)\varphi(y) - 32P_O P_O^-[P_A^+ \varphi^*(x)\varphi(y)$$
$$- P_A^* \varphi^*(x)\varphi^*(y)] + \text{c.c.} \quad \text{(B6)}$$

Other contributions, Fig. 6(e), 6(d), 6(i), 6(g) can be obtained by substituting $P_O \leftrightarrow P_A$, $P_A^+ \leftrightarrow -P_O^+$, $P_A^- \leftrightarrow -P_O^-$ in Eq. (B2), Eq. (B3), Eq. (B5), and Eq. (B6).

*Electronic mail: lidp@cc.nctu.edu.tw

†Electronic mail: baruch@vortex1.ep.nctu.edu.tw

[1] G. Blatter, M.V. Feigel'man, V.B. Geshkenbein, A.I. Larkin, and V.M. Vinokur, Rev. Mod. Phys. **66**, 1125 (1994).

[2] D.R. Nelson, Phys. Rev. Lett. **60**, 1973 (1988).

[3] E. Zeldov, D. Majer, M. Konczykowski, V.B. Geshkenbein, V.M. Vinokur, and H. Shtrikman, Nature (London) **375**, 373 (1995).

[4] M. Roulin, A. Junod, A. Erb, and E. Walker, J. Low Temp. Phys. **105**, 1099 (1996); A. Schilling *et al.*, Phys. Rev. Lett. **78**, 4833 (1997); S.W. Pierson and O.T. Valls, Phys. Rev. B **57**, R8143 (1998).

[5] D.J. Thouless, Phys. Rev. Lett. **34**, 946 (1975); G.J. Ruggeri and D.J. Thouless, J. Phys. F: Met. Phys. **6**, 2063 (1976).

[6] G.J. Ruggeri, Phys. Rev. B **20**, 3626 (1979).

[7] T. Barnes and G.I. Ghandour, Phys. Rev. D **22**, 924 (1980); A. Kovner and B. Rosenstein, *ibid.* **39**, 2332 (1989); **40**, 504 (1989).

[8] N.K. Wilkin and M.A. Moore, Phys. Rev. B **47**, 957 (1993).

[9] D. Li and B. Rosenstein, Phys. Rev. Lett. **86**, 3618 (2001).

[10] D. Li and B. Rosenstein, preceding paper, Phys Rev. B **65**, 024513 (2001).

[11] B. Rosenstein, Phys. Rev. B **60**, 4268 (1999).

[12] H.C. Kao, B. Rosenstein, and J.C. Lee, Phys. Rev. B **61**, 12 352 (2000). Note that in this reference the one loop coefficient is missing ω.

[13] One might object on the basis of Mermin–Wagner theorem, N.D. Mermin and H. Wagner, Phys. Rev. Lett. **17**, 1133 (1966), that in 2D the gauge U(1) and translation symmetry cannot be broken spontaneously. We address this concern below. The situation is similar to the one encountered while directly expanding energy in $1/a_T$ recently performed by one of us to the two loop order. Although the vortex solid state has only a quasi-long-range order rather than infinite-long-range order, in certain sense the state is much closer to the Gaussian solid state defined in this paper than to the Gaussian liquid state used in the high temperature perturbative expansion.

[14] Z. Tesanovic and A.V. Andreev, Phys. Rev. B **49**, 4064 (1994); Z. Tesanovic, L. Xing, L. Bulaevskii, Q. Li, and M. Suenaga, Phys. Rev. Lett. **69**, 3563 (1992).

[15] D. Li and B. Rosenstein, Phys. Rev. B **60**, 9704 (1999).

[16] D. Li and B. Rosenstein, Phys. Rev. B **60**, 10 460 (1999).

[17] D.J. Thouless, Phys. Rev. Lett. **34**, 946 (1975); A.J. Bray, Phys. Rev. B **9**, 4752 (1974).

[18] S. Hikami, A. Fujita, and A.I. Larkin, Phys. Rev. B **44**, R10 400 (1991); E. Brezin, A. Fujita, and S. Hikami, Phys. Rev. Lett. **65**, 1949 (1990); **65**, 2921 (1990).

[19] Y. Kato and N. Nagaosa, Phys. Rev. B **48**, 7383 (1993); J. Hu and A.H. Macdonald, Phys. Rev. Lett. **71**, 432 (1993); J.A. ONeill and M.A. Moore, Phys. Rev. B **48**, 374 (1993).

[20] V. Zhuravlev and T. Maniv, Phys. Rev. B **60**, 4277 (1999).

[21] G. Eilenberger, Phys. Rev. **164**, 628 (1967).

[22] K. Maki and H. Takayama, Prog. Theor. Phys. **46**, 1651 (1971).

[23] A. Lopatin and G. Kotliar, Phys. Rev. B **59**, 3879 (1999).

[24] M.A. Moore, T.J. Newman, A.J. Bray, and S.-K. Chin, Phys. Rev. B **58**, 9677 (1998).

[25] H. Kleinert, *Path Integrals in Quantum Mechanics, Statistics, and Polymer Physics* (World Scientific, Singapore, 1995).

[26] J.M. Cornwall, R. Jackiw, and E. Tomboulis, Phys. Rev. D **10**, 2428 (1974); R. Ikeda, J. Phys. Soc. Jpn. **64**, 1683 (1994); **64**, 3925 (1995).

[27] Note that similar simplification occurs in the large N approach developed in Ref. 23. Consequently their Anzatz is in fact a rigorous solution to their gap equations.